Promising emission behavior in Pr^{3+} / In selenide-chalcogenide-glass small-core step index fiber (SIF)

Hesham Sakr[a,b], Zhuoqi Tang[a], David Furniss[a], Lukasz Sojka[a], Slawomir Sujecki[a], Trevor M. Benson[a], and Angela B. Seddon*[,a].

[a] Mid-Infrared Photonics Group, George Green Institute for Electromagnetics Research, Faculty of Engineering,
University Park, University of Nottingham, Nottingham NG7 2RD, UK
[b] University of Science and Technology at Zewail City, Sheikh Zayed District, 6th of October City, Giza, Egypt.

*angela.seddon@nottingham.ac.uk

Abstract

Selenide-chalcogenide glass, small-core, step-index fiber (SIF), core-doped with Pr^{3+}: 9.51 x 10^{24} ions m^{-3} (500 ppmw) is fabricated for the first time with indium to help solubilize Pr^{3+}. Core diameters of 20 or 40 µm are confirmed using scanning electron microscopy and near-field imaging; fibre numerical aperture is ~0.4. Optical loss is ≥4.9 dB m^{-1} across the 3-9µm mid-infrared (MIR) spectral range. On pumping at 1.55 µm or 2.013 µm, the SIFs give broad MIR emission across 3.5-6 µm assigned to $^3H_6 \rightarrow {}^3H_5$ and $^3H_5 \rightarrow {}^3H_4$. The Pr^{3+} emission-lifetime at 4.7 µm decreases from *bulk*-glass (10.1 ±0.3 ms), to *intermediately* processed fiber (8.10 ±0.5 ms) to SIF (7.1 ±0.5 ms) induced by the processing. On end-pumping SIFs at 2.013 µm, the output pump-power and emission intensity at 4.7 µm became sub-linear and super-linear, respectively, suggesting MIR excited-state saturation is occurring.

KEYWORDS

mid-infrared, chalcogenide glass, rare earth ions, emission, emission-lifetime, excited-state saturation.

1. Introduction

The mid-infrared (MIR) spectral region spans the 3-50 μm spectral range [1]. MIR sources include blackbodies (*e.g. Globar*©), but these display low brightness. In contrast, MIR quantum cascade lasers, an emerging technology, and MIR OPOs (*optical parametric oscillators*) and gas (HeNe, CO, CO_2) lasers, which are mature technologies, exhibit high brightness. New MIR fiber narrow-line lasers are being developed along two strands: (i) nonlinear conversion, using stimulated Raman gain scattering [2] and (ii) direct-emission, rare earth ion (RE)-doped [3-6], - the topic of this study. MIR RE-doped fiber lasers have not yet been demonstrated at ≥4 μm [7], yet potentially offer advantages of compactness, high quantum efficiency, high brightness, excellent beam quality, ability to be pulsed, and greater reliability over gas lasers. MIR RE-doped fiber-lasers have prospective applications in providing new wavelengths for cutting/welding of soft materials, including polymers and in medical fiber-laser-surgery of human-tissue, and as narrow-line MIR molecular sensors [8]. Importantly, MIR RE-doped fiber lasers are potential pumps for MIR fiber supercontinuum (SC) laser sources to achieve all-fiber solutions for portable, real-time, broadband MIR molecular sensing, for instance for early diagnosis of cancer [8-15].

Chalcogenide glasses are promising RE hosts for MIR fiber-lasing due to their low phonon energy, large refractive indices hence large RE absorption/emission cross sections, long fluorescent-decay lifetimes [6] and potential for low optical-loss fiber-fabrication [see 16 and refs. therein]. Selenide-chalcogenide glasses, selected here, retain longer-wavelength near-infrared (NIR) transparency for pumping with commonly available lasers.

RE solubility is poor in binary chalcogenide glasses *e.g.* $As_{40}Se_{60}$ [17]. A Ga-solubilizer is commonly added to aid RE solubility in chalcogenide glasses [18] based on Ge-As/Sb-S/Se [18-23]. The RE solubility is considered to be enhanced by means of local [Ga-(S/Se)-RE] chemical-complexing [18]. We have made bulk selenide glasses doped with up to 6000 ppmw RE in the presence of Ga [24]. Also, with a Ga solubilizer, we have fabricated 500 ppmw Pr^{3+}/Ga small-core selenide-glass SIF (step-index fiber) which for the first time exhibited the same emission-lifetime at 4.7 μm as its parent bulk-glass - 7.8 ms [23]. This result implied that glass homogeneity was retained during the SIF glass-fabrication processing which was verified by a painstaking study to image and analyse the SIF small-core, and core/cladding interface, using high resolution transmission electron microscopy [23].

An In solubilizer was used to make a Pr^{3+}/In bulk selenide-chalcogenide glasses and large-core SIF [25-27]. In is in the same Group of the Periodic Table, as Ga, but heavier. Thus, potentially an [In-(S/Se)-RE] chemical-complex could offer a local, lower phonon energy environment to improve RE radiative-efficiency compared to the [Ga-(S/Se)-RE] chemical-complex, notwithstanding that RE 4f inner level transitions tend to be shielded from the local chemical environment. Indeed, on pumping at 1.55 μm, we found that the Pr^{3+} emission across 3.5-6 μm, and emission at 4.7 μm, were of greater intensity, and longer lifetime, respectively, in the Pr^{3+}/In bulk glass than in the Pr^{3+}/Ga bulk glass [25]. Further work on producing high

purity Pr^{3+} doped multi-component chalcogenide glasses can be found in [28-30], including the use of indium iodide to incorporate indium into Ge-As-Se-In-I [29] and Ge-Sb-Se-In-I [30] glasses.

Here, we report on a study of the emission behavior and fabrication for the first time of Pr^{3+}/In small-core SIFs based on selenide-chalcogenide glasses. The concentration of In solubilizer in the Pr^{3+}core was fixed at 1 atomic % (at. %). The SIF core-diameters were 20 μm and 40 μm, with a NA (numerical aperture) of ~ 0.4 (estimated from [23]) and V-parameter ~ 5.0, giving multi-moded behavior at 4-6 μm wavelength, corresponding to the $^3H_6 \rightarrow {}^3H_5$ and $^3H_5 \rightarrow {}^3H_4$ emissions and potential lasing emissions.

On pumping the SIF at 1.55 μm or 2.013 μm, broad MIR emission at 3.5-6 μm was observed. The Pr^{3+} emission-lifetime at 4.7 μm decreased from *bulk*-glass (10.1 ±0.3 ms), to *intermediately* processed fiber (8.10 ±0.5 ms) to SIF (7.1 ±0.5 ms); the decrease may have been induced by the processing. On end-pumping SIFs at 2.013 μm, the output pump-power collected from the opposite fiber-end to that pumped and emission intensity at 4.7 μm collected from same fiber-end to that pumped, became sub-linear and super-linear, respectively, suggesting MIR excited-state saturation is occurring for the first time in a chalcogenide-glass fiber.

2. Experimental

2.1 Bulk glass preparation

2.1.1 Cladding-glass boule (for extrusion to tube)

A Ge-As-In-Se-S cladding-glass boule (see Fig.1) was prepared. Ge (5n Materion), As (7n5 Furakawa Denshi, prior heat-treated at 10^{-3} Pa), indium (6n5 Alfa Aesar), Se (5n Materion, prior heat-treated at 10^{-3} Pa) and S (5N, prior boiled under 10^{-3} Pa for 5 mins) were batched inside a glovebox (MBraun: < 0.1 ppm H_2O and < 0.1 ppm O_2) and melted 850℃/8h in a silica glass ampoule (prior air-baked then vacuum-baked, each 1000℃/6h) before being quenched and annealed. 3 atomic% (at%) Se substitution by S manifested useful contrast in optical microscopic and SEM imaging; 1 at% Se replaced by S in chalcogenide glasses has been reported to reduce refractive index by 0.005 at 1.8 μm [31]. Glasses were annealed at the DSC *onset*-Tg [32].

2.1.2 Core-glass rod for caning and *intermediate* fiber-drawing

9.51×10^{24} ions m^{-3} (500 ppmw) Pr^{3+}-doped Ge-As-In-Se host core-glass (Fig.1) was prepared. First, Ge-As-Se was prepared as in section 2.1.1 and the glass transferred to a silica-glass still with 500 ppmw Al-wire (5N, Alfa Aesar: O-getter). The still was sealed under vacuum (10^{-3} Pa) and distillation executed within a two-zone furnace (Instron). The distilled Ge-As-Se was re-melted 800℃/7h, quenched, annealed and transferred to a new silica-glass ampoule (air-baked then vacuum-baked, each at 1000℃/6h) and re-melted with both indium (6n5 Alfa Aesar) and 500 ppmw Pr^{3+} (3n Alfa Aesar) for 6h/850℃ to form the doped core-glass rod. Again, glasses were annealed at the DSC *onset*-Tg [32].

2.2 Extrusion, caning, fiber-drawings and SIF fabrication

The extrusion, caning, fiber-drawings and SIF fabrication are depicted in processes (a), (b), (i) and (ii), respectively, in Fig. 1 :

(a) A melt-derived Ge-As-In-Se-S cladding-glass boule (from section 2.1.1) had an outside-diameter (OD) = 28.7 ± 0.1 mm and length (L) = 17 ± 0.1 mm.This boule was extruded [33] to give a cladding-tube (non-RE-doped Ge-As-In-Se-S) of OD = 10.5 ± 0.2 mm and ID (inner diameter) = 1.95 ± 0.05 mm (see Fig.1(a)).

(b) A melt-derived 9.51 x 10^{24} ions m^{-3} (500 ppmw) Pr^{3+}-doped Ge-As-In-Se core-glass rod (from section 2.1.2) was directly caned to give unclad cane of OD = 1.5 ± 0.1 mm (see Fig.1(b)).

(i) The melt-derived 9.51 x 10^{24} ions m^{-3} (500 ppmw) Pr^{3+}-Ge-As-In-Se core-glass rod (from section 2.1.2) was directly fiberised to give unclad *intermediate*-fiber, OD = 230 µm ± 20 µm (see Fig.1(i)).

(ii) The 9.51 x 10^{24} ions m^{-3} (500 ppmw) Pr^{3+}-Ge-As-In-Se unclad cane (see (b) above) was inserted in the Ge-As-In-Se-S cladding-tube (see (a) above) and then fiber-drawn as 'rod(b)-in-tube(a)' (under N_2 gas (BOC)) to make small-core SIF with 9.51 x 10^{24} ions m^{-3} (500 ppmw) Pr^{3+} doped Ge-As-In-Se core and undoped Ge-As-In-Se-S cladding, of core-OD as- designed/fiber OD = 20 µm / 130 µm and = 40 µm / 270 µm, respectively, (see Fig.1(ii)).

From now on, the term: 'Pr^{3+}/In small-core SIF' will be used to denote the two types of small-core SIFs each with 9.51 x 10^{24} ions m^{-3} (500 ppmw) Pr^{3+} doped Ge-As-In-Se core and undoped Ge-As-In-Se-S cladding, of core-OD as-designed/fiber OD = 20 µm / 130 µm or = 40 µm / 270 µm, respectively. Additionally, the term 'unstructured Pr^{3+}/In *intermediate* fiber' will be used to denote the unstructured fiber composed of 9.51 x 10^{24} ions m^{-3} (500 ppmw) Pr^{3+}-Ge-As-In-Se and of OD = 230 µm ± 20 µm (see Fig.1(i)).

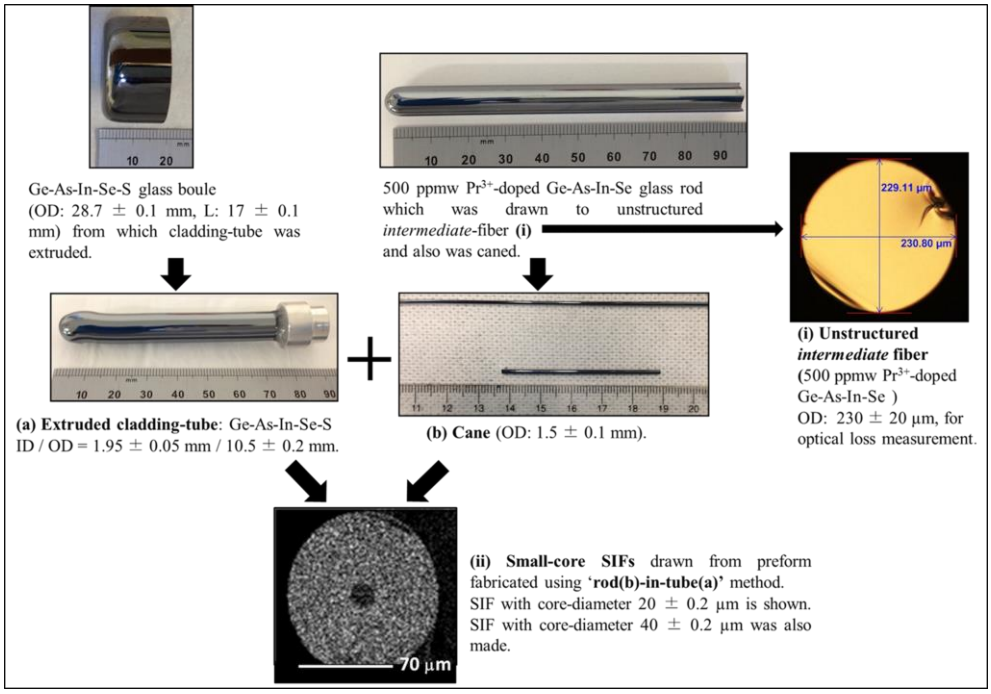

Fig. 1. Processing to produce 'Pr^{3+}/In small-core SIFs' (core/cladding = 500 ppmw Pr^{3+}-Ge-As-In-Se / Ge-As-In-Se-S, with as-designed 20 µm and 40 µm core diameters). OD is outside diameter.

2.3 Characterization of bulk glasses and fiber

2.3.1 Glass stability

Powder-XRD was done on samples to test for amorphicity in a Siemens Krystalloflex 810 X-ray diffractometer, with CuKα radiation, in the range 10 – 70 °2θ, in steps of 0.05 °2θ per 40 s with each XRD pattern collected in ~13 h.

2.3.1 Fiber optical loss

Optical loss of the 'unstructured Pr^{3+}/In *intermediate* fiber' (see Fig. 1(i)) was measured in the wavelength range 1 - 9 µm, using the cut-back method (detailed in [16]) with an IFS 66/S, Bruker Ft-MIR spectrometer and InGaAs, InSb and MCT detectors; the optical path was not purged. Fig. 2 shows the selected 'best' fiber cleaves used in the fiber-loss calculation.

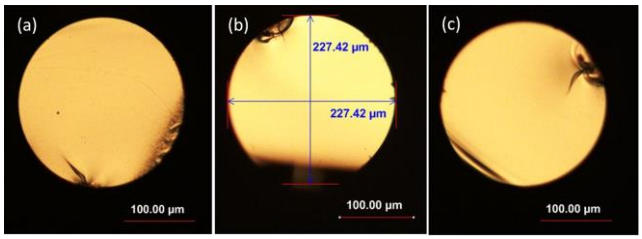

Fig. 2. (a) - (c) Optical micrographs of "best fiber-cleaves" used in fiber-loss calculation [16] of the 'unstructured Pr^{3+}-doped *intermediate* fiber' (see section 2.2, Fig. 1(i))

2.3.3 'Pr^{3+}/In small-core SIF' cross sectional geometry

The 'Pr^{3+}/In small-core SIFs' (Fig. 1(ii)) were analysed as follows. SIFs were cleaved, and cross sections carbon-coated then imaged and analysed by means of (E(environmental)) SEM-BSE and (E)SEM-EDX (FEG XL30 ESEM) with an Oxford Instruments INCA x-sight Si(Li) detector with ATW2 window.

Near-field, NIR imaging of 55-60 mm long samples was *via* a tunable laser: 1.465 – 1.575 µm (Agilent; 8164B). 1.465 µm was selected as being off-centre from the 1.45 µm Pr^{3+} absorption [23], with absorption falling sufficiently by 1.465 µm for detection of the guided light. The 1.465 µm light was launched into the 'Pr^{3+}/In small-core SIFs' using a tapered silica-fiber, mounted on a XYZ translation stage, with focused spot size 2.5 µm at the chalcogenide SIF launch-end. The output light was collected using a microscope x10 objective and collimated onto a Siemens XQ1112 vidicon tube camera.

2.3.4 Emission intensity and lifetime

A. Emission intensity

The Pr^{3+}-doped fiber was held on a XYZ optical-stage and pumped at 2.013 µm wavelength with a water-cooled, thulium fiber-laser, pumped at 793 nm (LISA Laser Products OHG, Germany). The emission from each Pr^{3+}-doped fiber was collected through a Spex MiniMate monochromator which had a diffraction-grating blazed at 6 µm. In order to increase the signal-to-noise ratio, the fluorescence signal was modulated using a chopper (95 Hz) and a lock-in amplifier was used (Brookdeal Electronics LTD 9503SC). The detection system was based on a room temperature MCT (mercury-cadmium-telluride) detector (Vigo

System PVI-6), preamplifier for the detector (Judson PA-6) and data acquisition card (NI USB-6008 National Instruments).

B. Emission lifetime

Fluorescent decay lifetimes at 4.7 μm were measured at RT using on /off modulation at 6.4 Hz of the pump laser and collected using different setups (Fig. 3), for instance the 'Pr^{3+}/In small-core SIFs', 145 mm long were end-pumped at 2.013 μm / 12 mW with collection at the same fiber-end as pumped (see Fig. 3(c)).

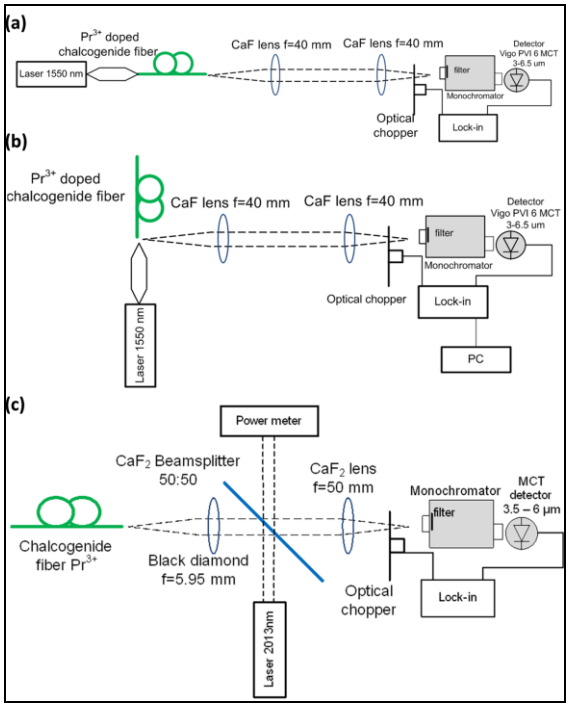

Fig. 3. Optical setups for measuring fiber photoluminescent (PL) intensity and lifetime (LT): collecting PL/LT from: (a) fiber-end opposite that pumped; (b) fiber-side and (c) from the same fiber-end as that pumped. Laser pump was 1.55 μm in (a) and (b), and 2.013 μm in (c).

For this, the pump light was passed through a collimator (Thorlabs), beam splitter (Thorlabs; Ø2" CaF_2 plate beamsplitter, coating: 2 - 8 μm, thickness = 3 mm) and chalcogenide-glass black-diamond lens (Thorlabs 390028-E; effective focal length 'EFL' = 5.95 mm); the diameter of the 2.013 μm wavelength excitation-beam after collimation was 2.2 mm and became 8.2 μm (~ circular) after focusing onto the end of the 'Pr^{3+}/In small-core SIFs' (core-diameters nominally 20 and 40 μm). In addition, end-collection of the 'Pr^{3+}/In small-core SIFs' was carried out at the opposite fiber end to that pumped when pumping at 1.55 μm. PL intensity and lifetimes were also measured in the 'Pr^{3+}/In *intermediate* fiber' (see Fig.1(i)) using end-collection at the opposite fiber end to that pumped (see Fig. 3(a)) and side-collection (see Fig. 3(b)) and pumping at 1.55 μm. Measurements were in ambient air and corrected for system response using a Globar© blackbody at 1430 K. Input pump-power was measured prior to launch into the Pr^{3+}-doped fibers, and on exit from the fiber, using a power-meter (Thorlabs; Thermal Sensors S302C).

3. Results and discussion

3.1 X-ray diffraction (XRD) crystallization study and optical loss spectra

XRD patterns (Fig.4) show amorphicity of: the Pr^{3+}/ In core-glass rod (see section 2.1.2, Fig.1), the undoped cladding-tube (section 2.2(a), Fig.1(ii)) and the Pr^{3+}/In unclad-cane (section 2.2(b), Fig.1(b)), although the XRD detection threshold is 2-5 vol.% of crystals [34]).

Fig.5 shows optical loss spectra spanning 1 - 9 µm of the 'unstructured Pr^{3+}/In *intermediate* fiber' (see section 2(i), Fig.1(i)). Fig. 5 also presents, for comparison purposes, the optical loss of a Pr^{3+}/In large-core *intermediate* SIF, reported previously in [25] (core / cladding = 498 ppmw Pr^{3+}-Ge-As-In-Se / Ge-As-In-Se of fiber OD = 270 ± 30 µm and core-diameter = 80-85% of fiber OD, formed by extrusion then fiber-drawing).

Fig.6 presents the electronic energy level diagram of an isolated Pr^{3+}-ion [35]. Comparing Figs.5 and 6, electronic absorption of Pr^{3+} is evident at 1.5 µm and 2 µm, assigned to transitions from the ground-state $^3H_4$ to two sets of degenerate excited-states ($^3F_4$, $^3F_3$) and ($^3F_2$, $^3H_6$), respectively. Absorption of Pr^{3+} centered at 4.5 µm is assigned as ground-state $^3H_4 \rightarrow {}^3H_5$; this masks underlying broad extrinsic absorption due to the glass impurity: [H-Se]- [6]. From Fig.5, further unwanted impurity extrinsic absorption bands are: -[O-H], [H-Se]-, [H-O-H], ≡[Ge-O]-/=[As-O]- and ≡[Si-O]- at 2.9, 3.5, 6.3, 7-7.9 and >9 µm, respectively. Loss spectra (Fig.5) indicate that the extra distillation steps followed here, compared to our earlier work [25], have reduced impurity-related absorption, especially: -[O-H], [H-O-H] and ≡[Ge-O]-/=[As-O]- peaks at 2.9, 6.3 and 7-7.9 µm, respectively. The minimum baseline optical loss of the 'unstructured Pr^{3+}/In *intermediate* fiber' (section 2.2 and Fig.1(i)) was 4.9 ± 0.3 dB/m at 6.84 µm, across 1-9 µm. These losses are higher than the best loss results to date for Pr^{3+} doped unstructured doped glass fiber, published recently in [28]. The results of [28] give confidence that background losses can be reduced to below the 1 dB m^{-1} limit that modeling suggests is desirable if efficient MIR fiber lasers are to be realized [36].

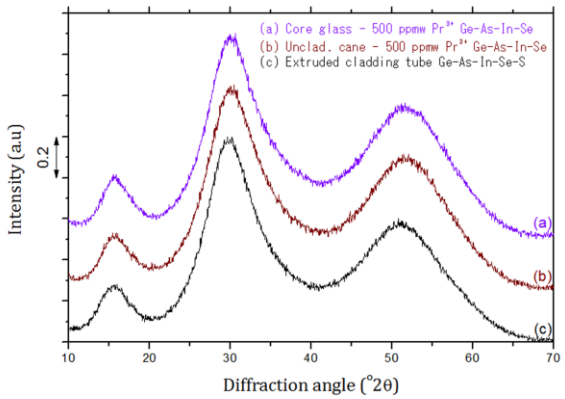

Fig. 4. XRD patterns of: (a) Pr^{3+}/ In core-glass rod (see section 2.1.2 and Fig.1); (b) Pr^{3+}/In unclad-cane (section 2.2(b) and Fig.1(b)) and (c) undoped cladding-tube (section 2.2(a) and Fig.1(ii)).

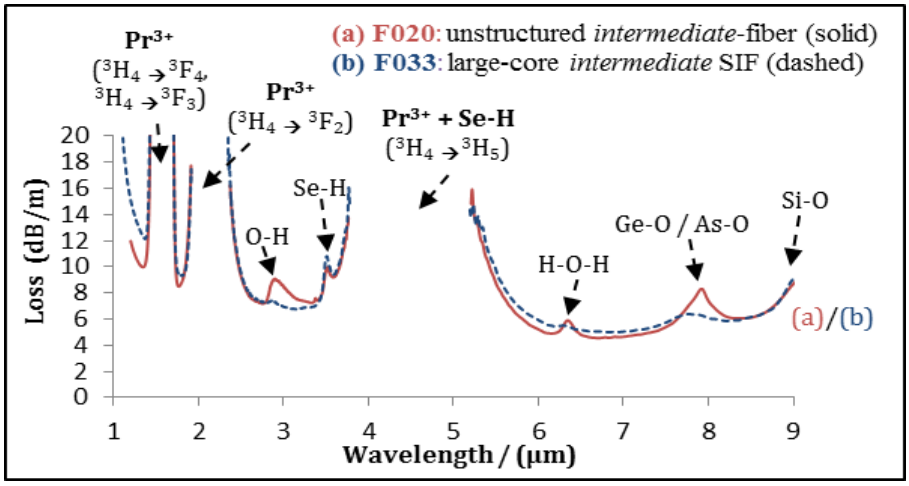

Fig. 5. Optical loss spectra across 1 - 9 µm of the 'unstructured Pr^{3+}/In *intermediate* fiber' (section 2.2 and Fig.1(i)), which underwent glass-distillation, compared to a Pr^{3+}/In large-core *intermediate* SIF, from previous work [25] (core /cladding = 498 ppmw Pr^{3+}-Ge-As-In-Se / Ge-As-In-Se (fiber OD = 270 ± 30 µm; core diameter = 80-85% fiber OD).

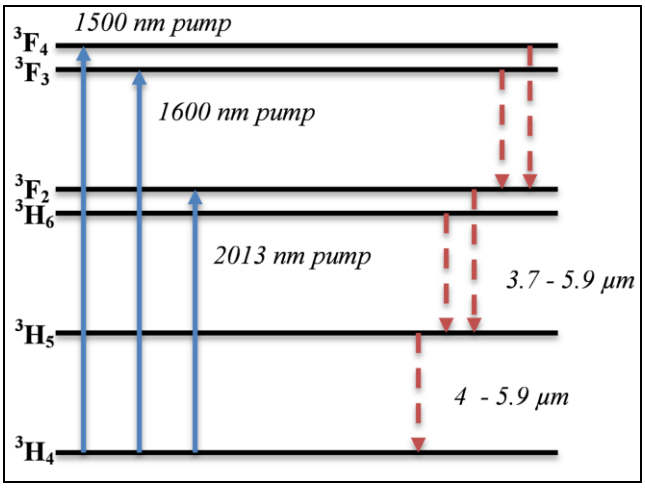

Fig. 6. Energy-level diagram of isolated Pr^{3+}-ion with absorptive transitions identified (from [31]) of interest here, together with potential longer-wavelength radiative transitions.

3.2 Near-field imaging and elemental mapping of the small-core SIF

Fig. 7 (a)-(e) show near-field imaging at 1.465 µm of the 'Pr^{3+}/In small-core SIFs' (see section 2.2, Fig.1(ii)). Figs. 7(a), (c) demonstrate cladding modes were guided and Fig. 7(e) confirms multi-modal guiding at 1.465 µm. Fig. 8 shows ESEM-EDX elemental mapping of In and S in the 'Pr^{3+}/In small-core SIFs' (see section 2.2, Fig.1(ii))). From Fig.8, the small cores were concentric, centralized and circular, and fabricated core-diameters were observed to be: (a) 19.8 ± 0.5 µm (*planned: 20 µm*) and (b) 39.4 ± 0.6 µm (*planned: 40 µm*).

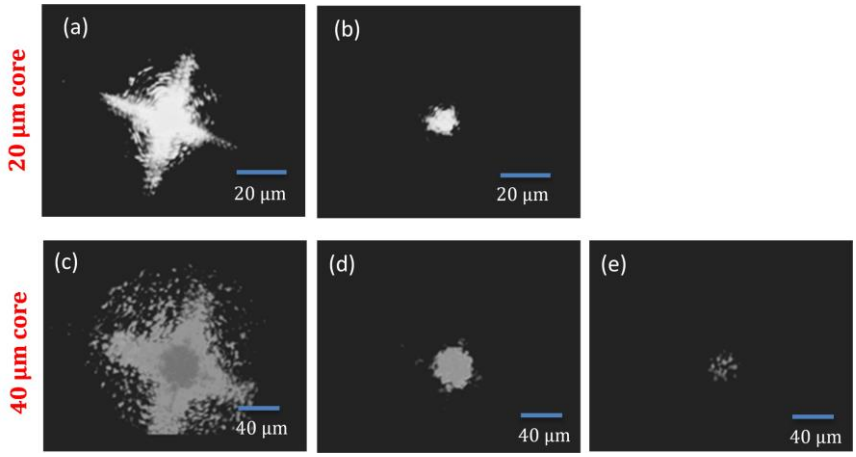

Fig. 7. Near-field images of guiding core at 1.465 µm and different launch-angles into multimoded 'Pr^{3+}/In small-core SIFs' (see section 2.2, Fig.1(ii)). (a), (b) 20 µm-diameter small-core SIF (55 mm long). (c), (d), (e) 40 µm-diameter small-core SIF (60 mm long)

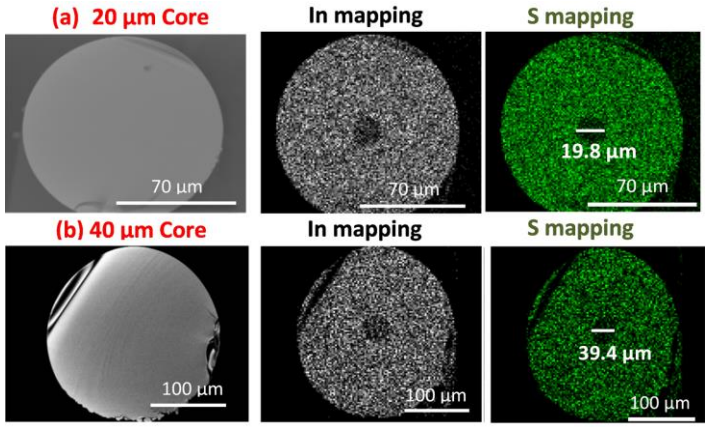

Fig. 8.(E)SEM-EDX elemental mapping of In, S in 'Pr^{3+}/In small-core SIFs' (see Fig.1(ii)) showing: (a) 19.8 ±0.5 µm core-diameter (designed 20 µm) and (b) 39.4 ± 0.6 µm core-diameter (designed 40 µm).

3.3 Emission in 'Pr^{3+}/In small-core SIFs'

Pr^{3+} absorption bands at 1.55 µm, 2.013 µm were selected for pumping (see Figs.5, 6). In Fig. 9, plot (a) is prior work [25]: emission in Pr^{3+}/In *bulk* glass (*melt-derived 531 ppmw Pr^{3+}-Ge-As-In-Se*) pumped at 1.55 µm/50.2 mW (orthogonal pump/collection across sharp corner, as in [25]), for comparison. Plot (b) is the normalized emission spectrum of the 20 µm core-diameter 'Pr^{3+}/In small-core SIF' (section 2.2, Fig.1(ii)) across 3.5-6 µm, when end-pumped at 2.013 µm / 25 mW, with emission collected from the same fiber-end as that pumped (as Fig. 3(c)). Under the same pump/collection conditions, the normalized emission from the 40 µm core-diameter 'Pr^{3+}/In small-core SIF' (section 2.2, Fig.1(ii)) overlaid this 3.5-6 µm emission (*not shown*). In the absence of evidence to the contrary, the 3.5-6 µm fluorescent emission is assigned to combined emissions: ($^3F_2$, $^3H_6 \rightarrow {}^3H_5$) and ($^3H_5 \rightarrow {}^3H_4$) (Fig.6) [37]. These transitions are radiative in selenide glass and non-radiative in fluoride glass [38] due to the high phonon energy of fluoride glasses. Fig.9 plots (c) and (d) are prior results for comparison [25], in a Pr^{3+}/In large-core *intermediate* SIF (*core/cladding = 498 ppmw Pr^{3+}-Ge-As-In-Se / Ge-As-In-Se, fiber OD = 270 ± 30 µm, core-diameter = 80-85% of fiber OD).* Plot (c) is side-collection (*cf.* Fig. 3(b)) with end-pumping at 1.55 µm/50.8 mW; plot (d)

is fiber-end collection (*cf.* Fig. 3(a)) at the opposite end from that pumped (at 1.55 µm/24.5 mW). Plot (d) is broadened relative to plot (c) at the low energy side of the spectral emission band, indicating that photon trapping [39] occurred when emission was collected at the fibre-end opposite to that pumped (as in Fig.3(a)) and less so when collected from the side of the fiber.

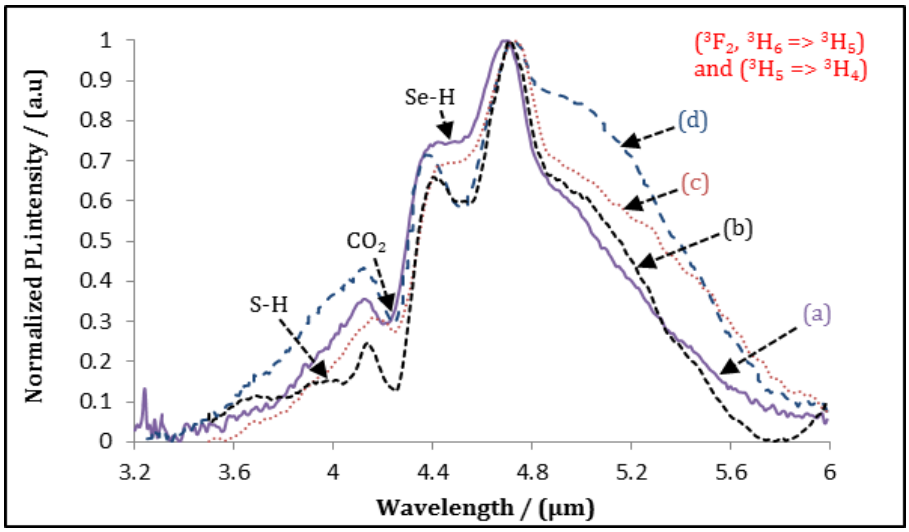

Fig. 9. Normalized fluorescence-emission at 3.5-6 µm: (a) prior work: *bulk* glass (531 ppmw Pr^{3+}-Ge-As-In-Se) with orthogonal pump (1.55 µm/50.2 mW), fluorescent-emission collection across a sharp corner [25]; (b) 20 µm core-diameter 'Pr^{3+}/In small-core SIF' (section 2.2, Fig.1(ii)) end-pumped at 2.013 µm /25 mW with fluorescent-emission collection from same fiber-end as pumped (*cf.* Fig. 3(c); (c) from prior work [25]: Pr^{3+}/In large-core *intermediate* SIF (core/cladding = 498 ppmw Pr^{3+}-Ge-As-In-Se/Ge-As-In-Se (fiber OD: 270 ± 30 µm, 80-85% core-diameter)) end-pumped at 1.55 µm/50.84 mW with fluorescent-emission collection at side of fiber (Fig. 3(b) and (d) fiber same as (c) [25], but end-pumped, at 1.55 µm / 24.5 mW with fluorescent-emission collection at *opposite end of fiber* to that pumped (Fig. 3(a).

Fig. 10(a) shows the variation in emission intensity at 4.7 µm, of the 20 µm and 40 µm core-diameter 'Pr^{3+}/In small-core SIFs (section 2.2, Fig.1(ii)), as a function of the input pump-power for end-pumping at 2.013 µm / 0-180 mW; emission was collected from the same fiber-end as that pumped (*cf.* Fig. 3(c)). Fig. 10(b) shows the variation in pump-power exiting the opposite end of the fiber to that pumped, for pumping 2.013 µm / 20-180 mW of 20 µm and 40 µm core-diameter 'Pr^{3+}/In small-core SIFs' (section 2.2, Fig.1(ii)) as a function of the input pump-power. From Fig. 10, both fibers show an approximate linear increase in emission intensity at 4.7 µm exiting the same fiber-end as that pumped, and pump-power exiting the fiber-end opposite to that pumped, with increasing input pump-power from 10-80 mW. However, from 80-170 mW pump-power, the emission intensity and pump-power exiting the pumped fiber became nonlinear: the emission intensity response became super-linear and the pump-power exiting response became sub-linear.

We suggest this behavior could be related to bleaching of the electronic ground state ($^3H_4$, Fig. 6), thereby limiting further pump absorption [40] and maybe evidence of approaching saturation of an excited state. Fluorescent peak intensity of RE-ions would normally start to saturate as an population-inversion is approached. We have found no reports of similar nonlinear behavior in the literature for MIR fluorescent-emission at greater than 3.9 µm [7], nor pump-power exiting, in RE-ion doped glass fibers. It is not claimed that a population-inversion has been achieved here and gain would have been suppressed by the presence of

resonant extrinsic absorption, and possibly extrinsic non-radiative decay, [6, 41] due to [H-Se-]- impurity, oxide and other impurities in the host. Our prior work, and that of others, has shown that ultra-low optical loss of undoped chalcogenide glass fibers may be achieved [16 and refs. therein]. Here, the Pr^{3+}-dopant and In solubilizer have brought into the glass-host extra unwanted impurities and raised the optical loss in the fiber [42].

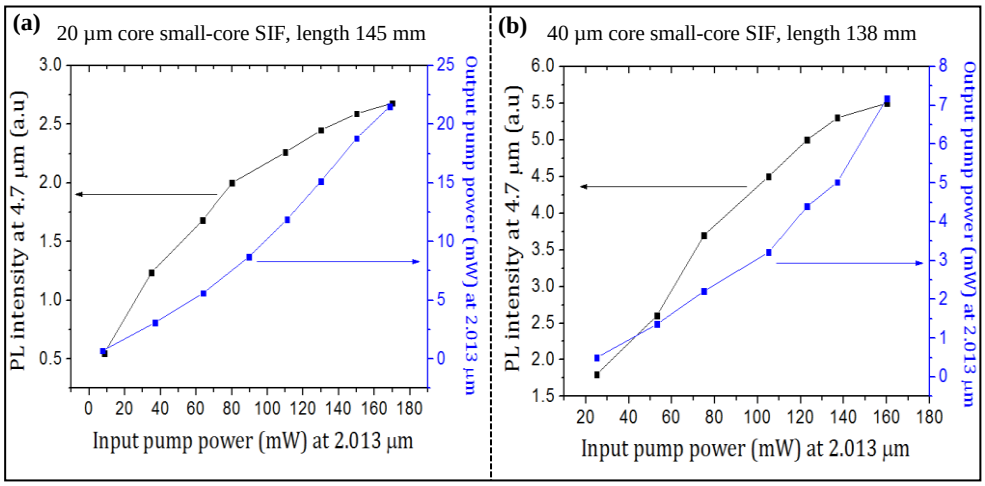

Fig. 10. For end-pumping at 2.013 µm: (a) 20 µm core-diameter 'Pr^{3+}/In small-core SIF' (section 2.2, Fig.1(ii)) and (b) 40 µm core-diameter 'Pr^{3+}/In small-core SIF' (section 2.2, Fig.1(ii)). Plotted for each of (a) and (b) are the output pump-power collected from the opposite fiber end to that pumped (*blue solid squares*), and fluorescent-intensity at 4.7 µm collected from the same fiber-end as that pumped (*black solid squares*) (see Fig.3(c)), plotted as a function of the incident input pump-power.

3.4 Fluorescent-lifetimes

Table 1 collates the fluorescent-lifetimes of the 'Pr^{3+}/In *intermediate* fiber and small-core SIFs' (section 2.2, Fig.1(ii) and (ii), respectively) at 4.7 µm wavelength, when pumping at 1.55 µm or 2.013 µm compared to 'Pr^{3+}/In bulk-glass' from prior work [25].

From Table 1, the Pr^{3+} fluorescent-lifetime at 4.7 µm in the presence of an In solubilizer tends to decrease from *bulk* glass (10.1 ± 0.3 ms) [25], to *intermediate* fiber (8.0-8.2 0.5 ms) to small-core SIFs (7.1 ± 0.5 ms). This decrease in lifetime for Pr^{3+}/In samples is in contrast to Pr^{3+}/Ga samples, for which the Pr^{3+} fluorescent-lifetime at 4.7 µm, when pumped at 1.55 µm, of 7.8 ± 0.3 ms for *bulk*-glass was maintained in small-core SIFs [23]).

Below, we argue that the decrease in Pr^{3+} fluorescent-lifetime in the presence of an In solubilizer goes hand-in-hand with an increase in the cumulative-processing required to prepare each type of sample.

Processing is required to achieve shaping of preforms, cane, tubes and fiber. Each processing-step here comprised a heat-treatment where the glass was heated to some temperature between T_g and the liquidus, in the supercooled-liquid regime, for shaping to take place, followed by cooling to ambient. In cases other than caning or fiberizing, an isothermal-hold took place at T_g during the cooling- step in order to anneal the glass and abolish permanent stress. The supercooled-liquid is thermodynamically metastable and tends to lower free energy by undergoing nucleation then crystallisation. Accompanying this phase change (or pre-phase-change, in the case of glass nucleation) there may be a tendency for RE-ions in the melt to cluster. Any

nucleation, crystallisation or clustering 'frozen-in' on cooling to T_g, could ultimately lead to concentration-quenching of the excited states of the RE-ions.

Shaping of the supercooled liquid takes time, and concurrent nucleation/ crystallisation/clustering depends on the degree of undercooling during shaping, which influences not only the nucleation rate but also the supercooled liquid viscosity which is the macroscopic manifestation of the kinetic limitations to phase change and to clustering influencing the time-taken for atomic-diffusion. In a nutshell, during processing-steps, it is the cumulative time of visits to the supercooled liquid (heating, cooling or isothermal hold) which eventually leads to a non-homogeneous glass at ambient temperature.

From Table 1, labeled *(I)*, the Pr^{3+}/In bulk glass (Pr^{3+}-Ge-As-In-Se [25]) exhibited the longest lifetime of all samples (10.1 ±0.3ms); the glass was melted above the liquidus (where there is no thermodynamic tendency for devitrification or clustering) then cooled through the supercooled-liquid regime to T_g, annealed and cooled to ambient. In short, this sample received processing comprising {1x cooling} through the supercooled-liquid range.

Table 1. Pr^{3+} fluorescent-lifetime, in the presence of In, at 4.7 μm in bulk glass, *intermediate* fiber and small-core SIF, arranged vertically downwards in order of decreasing PL lifetime (column 2), with details of samples and measurement setups. (Key: SIF: step index fiber, N/A not applicable, OD: outer diameter, λ: wavelength.)

Pr^{3+}-doped with In solubilizer: sample type.	**PL lifetime /ms**	**Pumped at λ / μm. (Power/mW)**	**Pump launch.**	**PL collection set-up.**	**• [Pr^{3+}]/ ppmw. • Glass host. • (Cladding glass)**	**Sample geometry.**
***(I)* Bulk glass** [25]	**10.1±0.3**	1.55 (57.8)	1 mm from sharp corner.	1 mm from sharp corner, orthogonal to pump.	• **531** • Ge-As-In-Se • (N/A)	Polished sharp corner.
***(II)* Unstructured *intermediate* fiber**	**8.0 ±0.5**	1.55 (50.8)	″	Fiber side (orthogonal to pump) Fig.3(b).	• **500** • Ge-As-In-Se • (N/A)	Fiber OD 230 ±20 μm. (section 2.2, Fig.1(i)).
	8.2 ±0.3	″	″	Fiber end (opposite to pump) Fig.3(a).		
***(III)* Small-core SIF**	**7.2 ±0.5**	1.55 (2.2)	″	Fiber end (opposite to pump) Fig.3(a).	• **500** • Ge-As-In-Se • **(**Ge-As-In-Se-S)	Core OD 20 μm. Fiber OD 130 ±10 μm (section 2.2, Fig.1(ii)).
	7.0 ±0.1	2.103 (12.0)	″	Fiber end (same end as pump) Fig.3(c).		

The 'unstructured Pr^{3+}/In *intermediate* fiber' (section 2.2, Fig.1(i)), labeled (*II*) in Table 1, was drawn directly from a melted, quenched, annealed Pr^{3+}-doped glass rod. In short, this sample received processing

comprising: {(1x (cooling) then 1x (heating/cooling)} in the supercooled-liquid regime. The fiber fluorescent-lifetimes measured by side- and end-collection agreed.

The 20 μm core-diameter 'Pr^{3+}-doped small-core SIF' (section 2.2, Fig.1(ii), sample *IV* in Table 1) had the shortest fluorescent-lifetimes (7.1 ±0.5 ms) of all samples and underwent the most intricate fabrication processing, consisting of: (i) melting, quenching and annealing of the Pr^{3+}-doped core and undoped cladding glasses followed by: (ii) cane-drawing Pr^{3+}-doped core-glass; (ii) placing Pr^{3+}-doped cane in the undoped cladding tube (made by extruding the undoped-cladding glass) and fiber-drawing 'rod-in-tube' (see Fig.1(ii)). The core/cladding interface was formed during the fiberizing. In short, this sample received processing comprising: {1x (cooling) then 2x (heating/cooling)} in the supercooled-liquid regime.

We speculate that the processing to form the SIF may have caused some Pr^{3+} clustering and/or glass-nucleation/crystal growth. We showed earlier [25] that Pr^{3+}/In selenide bulk-glasses have more tendency than their Pr^{3+}/Ga counterparts to devitrify at ≥1000 ppmw Pr^{3+}. An increase in light scattering loss accompanying loss of glass homogeneity could not be studied in the small-core SIF by direct optical-loss measurement due to the too large étendue of the MIR blackbody source available for measuring broadband loss.

It is important to note that the measured Pr^{3+} lifetimes in Table 1 may be of a subset of Pr^{3+} ions that are not quenched by, [H-Se]- or -[O]- impurities [6, 41].

Potential radiative mechanisms include that during excitation, pump upconversion could have occurred, due to potential resonance of the 2.013 μm pump-laser and the energy absorptive process $^3H_5 \rightarrow {}^3F_3$ of Pr^{3+}, after initial pumping to [$^3F_2$, $^3H_6$] followed by radiative emission: $^3H_6 \rightarrow {}^3H_5$. The $^3H_5$ level could also have been depopulated through this process. Further, 2.013 or 1.55 μm pumping could incur cross-relaxation between neighbouring Pr^{3+} ions: $^3H_6 \rightarrow {}^3H_5$ could have caused excitation upconversion of $^3H_6 \rightarrow {}^3F_3$. In which case, emission could also have been contributing from $^3F_3 \rightarrow {}^3H_4$, known to lase at 5.2 μm in Pr^{3+}-doped chloride crystals [43]. From Table 1, the measured lifetimes of the 'Pr^{3+}/In small-core SIFs' were the same for 1.55 μm or 2.013 μm pumping. This suggests that the levels $^3H_6$ and $^3H_5$ are depopulated in a similar manner, whether pumping at 1.55 μm or 2.013 μm. Thus, 2.013 μm pump-upconversion was probably minimized, at least for this doping concentration.

4. Conclusions

20 and 40 μm core diameter SIFs, with core / cladding = 9.51 x 10^{24} ions m^{-3} (500 ppmw) Pr^{3+} doped Ge-As-In-Se / Ge-As-In-Se-S, have been fabricated with NA ~0.4 (estimated from [23] and multimode operation at 4-6 μm, encompassing potential lasing wavelengths. Each core was circular and centralized, and of diameter close to the design. NIR light-guiding in the SIF core was demonstrated. The lowest possible SIF optical loss, across 3-9 μm was 5 dB m^{-1} at 6.84 μm The SIF fluorescent-emission spanned 3.5-6 μm, when end-pumped at at 2.013 μm. The fluorescent-decay lifetime at 4.7 μm wavelength of the 20 μm core fiber (7.1 ±0.5 ms) was lower than that found in *intermediate* fiber (8.1 ±0.5 ms) or in bulk glass (10.1 ±0.3 ms, [25]). This trend appears to be related to the number of processing-steps to fabricate SIF causing potential decrease in glass homogeneity and some greater ordering around, or of, the doped-in Pr^{3+}. (This result is in contrast to

analogous Pr^{3+}/ Ga selenide-glass small-core SIF which was shown, in earlier work [23], to maintain the same PL lifetime (7.8 ± 0.3 ms) in SIF as in the parent *bulk*-glass.) When end-pumping the 20 and 40 µm core-diameter Pr^{3+}/In SIFs at 2.013 µm / 80-170 mW, the Pr^{3+} fluorescent emission intensity, and residual pump-power, exiting the SIFS became super-linear, and sub-linear, respectively, as the pump-power was increased from 80-170 mW. These trends for the first time suggest MIR excited-state saturation of a Pr^{3+}-dopant in a chalcogenide fiber.

5. Acknowledgments

This research was in part supported by the European Commission through Framework Seven (FP7) project MINERVA MId- to NEaR infrared spectroscopy for improVed medical the diAgnostics (317803; www.minerva-project.eu). The Author, Hesham Sakr, thanks the University of Nottingham, UK, for a PhD Scholarship.

6. References

[1] BSI ISO 20473:2007 Optics and photonics. Spectral bands. 2007, checked 2015, BSI. p. 10. (British Standards Institution (BSI) and International Organization for Standardization (ISO).) Consulted September 2016.

[2] M. Bernier, V. Fortin, M. El-Amraoui, Y. Messaddeq, R. Vallée, 3.77µm fiber laser based on cascaded Raman gain in a chalcogenide glass fiber, Opt. Lett. 39(7) (2014) 2052-2055.

[3] F. Charpentier, F. Starecki, J. L. Doualan, P. Jóvári, P. Camy, J. Troles, S. Belin, B. Bureau, V. Nazabal, Mid-IR luminescence of Dy^{3+} and Pr^{3+} doped $Ga_5Ge_{20}Sb_{10}S(Se)_{65}$ bulk glasses and fibers, Mater. Lett. 101, (2013) 21-24.

[4] B. Cole, L. B. Shaw, P. C. Pureza, R. Miklos, J. S. Sanghera, I. D. Aggarwal, Core/clad selenide glass fiber doped with Pr^{3+} for active MIR applications, J. Mater. Sci. Lett. 20 (5) (2000) 465–467.

[5] S. D. Jackson, Towards high-power mid-infrared emission from a fiber laser, Nat. Photonics 6 (2012) 423–431.

[6] A. B. Seddon, Z. Tang, D. Furniss, S. Sujecki, T. M. Benson, Progress in rare-earth-doped mid-infrared fiber lasers, Opt. Express 18 (25) (2010) 26704-26719.

[7] J. Schneider, "Fluoride fiber laser operating at 3.9 µm", Electronic Letters 31(15), (1995), 1250-1251.

[8] A. B. Seddon, Mid-infrared optical sensing and imaging, in: Springer Handbook of Glass, J.D. Musgraves, J. Hu, L. Calvez (Eds.) (Springer, in press).

[9] A. B. Seddon, A prospective for new mid-infrared medical endoscopy using chalcogenide glasses, Int. J. Appl. Glass Sci. 2(3) (2011) 177–191.

[10] A. B. Seddon, Mid-infrared (IR) – A hot topic: The potential for using mid-IR light for non-invasive early detection of skin cancer in vivo, Phys. Status Solidi B. 250(5), (2013) 1020–1027.

[11] A. B. Seddon, Biomedical Applications in Probing Deep Tissue using Mid-Infrared (MIR) Supercontinuum Optical Biopsy, in: R.R. Alfano, L. Shi (Eds.), Deep Imaging in Tissue and Tissue-Like Media with Linear and Nonlinear Optics (Pan Stanford Publishing, in press)

[12] A. B. Seddon, B. Napier, I. Lindsay, S. Lamrini, P. M. Moselund, N. Stone, O. Bang, Mid-infrared spectroscopy/bioimaging: moving towards MIR optical biopsy, BioOptics World 2 February 2016.

[13] C. R. Petersen, U. Moller, Irnis Kubat, B. Zhou, S. Dupont, J. Ramsay, T. Benson, S. Sujecki, N. Abdel-Moneim, Z. Tang, D. Furniss, A. Seddon, O. Bang Mid-infrared supercontinuum covering the 1.4–13.3 µm molecular fingerprint region using ultra-high NA chalcogenide step-index fiber, Nat. Photonics 8 (2014) 830-834 (Please see [14]).

[14] G. Steinmeyer, J. S. Skibina, Entering the mid-infrared: the demonstration of chalcogenide fiber-based supercontinuum sources that reach beyond a wavelength of ten micrometres is set to have a major impact on spectroscopy and molecular sensing, Nat. Photonics News and Views 8 (2014) 814-815. (Please see [13].)

[15] B. Zhang, Y. Yu, C. Zhai, S. Qi, Y. Wang, A. Yang, X. Gai, R. Wang, Z. Yang, B. Luther-Davies: High brightness 2.2-12 µm mid-infrared supercontinuum generation in a nontoxic chalcogenide step-index fiber, J. Am. Ceram. Soc. 99(8) (2016) 2565-2568.

[16] Z Tang, V. S. Shiryaev, D. Furniss, L. Sojka, S. Sujecki, T. M. Benson, A. B. Seddon, M. F. Churbanov, Low loss Ge-As-Se chalcogenide glass fiber, fabricated using extruded preform, for mid-infrared photonics, Opt. Mater. Express 5(8) (2015) 1722-1737.
[17] M. S. Iovu, S. F. Shutov, A. M. Andriesh, E. J. Kamitsos, C. P. E Varsamis, D. Furniss, A. B. Seddon, M. Popescu, Spectroscopic studies of bulk As2S3 glasses and amorphous films doped with Dy, Sm, and Mn, J. Optoelect. Adv. Mat. 3(2) (2001) 443-454.
[18] G. Aitken, C. W. Ponader, R. S. Quimby, Clustering of rare earths in GeAs sulfide glass, Compt. Rend. Chim. 5(12) (2002) 865–872.
[19] J. Park, H. S. Seo, J. T. Ahn, Y. G. Choi, D. Y. Jeon, W. J. Chung, Mid-infrared (3.5-5.5 μm) spectroscopic properties of Pr^{3+}-doped Ge-Ga-Sb-Se glasses and optical fibers, J. Lumin. 128(10) (2008) 1617-1622.
[20] L. B. Shaw, B. Cole, D. T. Schaafsma, B. B. Harbison, J. S. Sanghera, I. D. Aggarwal, Rare-earth-doped selenide glass optical sources, in Lasers and Electro-Optics, CLEO 98 Tech. Digest. (1998), pp. 420-421.
[21] B. Cole, L. B. Shaw, P. C. Pureza, R. Mossadegh, J. S. Sanghera, I. D. Aggarwal, Rare-earth doped selenide glasses and fibers for active applications in the near and mid-IR, J. Non-Cryst. Solids 256&257, (1999) 253-259.
[22] L. Sójka, Z. Tang, D. Furniss, H. Sakr, A. Oladeji, E. Bereś-Pawlik, H. Dantanarayana, E. Faber, A. B. Seddon, T. M. Benson, S. Sujecki, Broadband, mid-infrared emission from Pr3+ doped GeAsGaSe chalcogenide fiber, optically clad, Opt. Mater. 36(6) (2014) 1076-1082.
[23] Z. Tang, D. Furniss, M. Fay, H. Sakr, L. Sójka, N. Neate, N. Weston, S. Sujecki, T. M. Benson, A. B. Seddon, Mid-infrared photoluminescence in small-core fiber of praseodymium-ion doped selenide-based chalcogenide glass, Opt. Mater. Express 5(4 (2015) 870–886.
[24] Y. Cheng, Z. Tang, N. C. Neate, D. Furniss, T. M. Benson, A. B. Seddon, The influence of dysprosium addition on the crystallization behavior of a chalcogenide selenide glass close to the fiber drawing temperature, J. Am. Ceram. Soc. 95(12) (2012) 3834-3841.
[25] H. Sakr, D. Furniss, Z. Tang, L. Sojka, N. A. Moneim, E. Barney, S. Sujecki, T. M. Benson, A. B. Seddon, Superior photoluminescence (PL) of Pr^{3+}-In, compared to Pr^{3+}-Ga, selenide-chalcogenide bulk glasses and PL of optically-clad fiber, Opt. Express 22 (2014) 21236-21252.
[26] H. Sakr, Z. Tang, D. Furniss, L. Sojka, N. A. Moneim, E. Barney, S. Sujecki, T. M. Benson, A. B. Seddon, Towards mid-infrared fiber-lasers: rare earth ion doped, indium-containing, selenide bulk glasses and fiber, Proc. SPIE 8938 (2014) 89380V-1.
[27] D. Furniss, H. Sakr, Z Tang, S. Sujecki, E. Barney, T. M. Benson, A. B. Seddon, Development of praseodymium-doped, selenide chalcogenide glass, step-index fibre towards mid-infrared fibre lasers, in Proc. 18th International Conference on Transparent Optical Networks (2016).
[28] E.V. Karaksina, V.S. Shiryaev, T.V. Kotereva, A.P. Velmuzhov, L.A. Ketkova, G.E. Snopatin, Preparation of high-purity Pr3+ doped Ge–As–Se–In–I glasses for active mid-infrared optics, J. Lumin. 177 (2016) 275–279
[29] E.V. Karaksina, V.S. Shiryaev, T.V. Kotereva, M.F. Churbanov, Preparation of high-purity Pr(3+) doped Ge–Ga–Sb–Se glasses with intensive middle infrared luminescence, J. Lumin. 170 (2016) 37–41
[30] V.S. Shiryaev, E.V. Karaksina, T.V. Kotereva, M.F. Churbanov, A.P. Velmuzhov, M.V. Sukhanov, L.A. Ketkova, N.S. Zernova, V.G. Plotnichenko, V.V. Koltashev, Preparation and investigation of Pr3+-doped Ge–Sb–Se–In–I glasses as promising material for active mid-infrared optics, J. Lumin. 183 (2017) 129–134
[31] L. G. Aio, A. M. Efimov, V. F. Kokorina, Refractive index of chalcogenide glasses over a wide range of compositions, J. Non-Cryst. Solids 27 (1978) 299-307.
[32] D. Furniss, A. B. Seddon, Principles and Applications of Thermal Analysis, Ed. Paul Gabbott, (Blackwells, 2007), Chap. 10.
[33] S. D. Savage, C. A. Miller, D. Furniss, A. B. Seddon, Extrusion of chalcogenide glass preforms and drawing to multimode optical fibers, J. Non-Cryst. Solids 354(29) (2008) 3418–3427.
[34] Z. Tang, N. C. Neate, D. Furniss, S. Sujecki, T. M. Benson, A. B. Seddon, Crystallization behavior of Dy3+- doped selenide glasses, J. Non-Cryst. Solids 357(11–13) (2011) 2453-2462.
[35] H. Dieke, H. M. Crosswhite, The spectra of the doubly and triply ionized rare earth, Appl. Optics 2 (1963) 675-686.
[36] Ł. Sójka, Z. Tang, H. Zhu, E. Bereś-Pawlik, D. Furniss, A. B. Seddon, T. M. Benson, S. Sujecki, Study of mid-infrared laser action in chalcogenide rare earth doped glass with Dy^{3+}, Pr^{3+} and Tb^{3+}, Opt. Mat. Expr. 2 (11) (2012) 1632-1640.

[37] M. Walsh, H. R. Lee, N. P. Barnes, Mid-infrared lasers for remote sensing applications, J. Lumin. 169 (2016), 400-405.

[38] F. Z. Qamar, T.A. King, S. D. Jackson, Y. H. Tsang, Holmium, praseodymium doped fluoride fibre laser operating near 2.87 μm and pumped with an Nd-YAG laser, J. Lightwave Technol. 23(12) (2005) 4315-4320.

[39] S. Kasap, C. Koughia, The influence of radiation trapping on spectra and measured lifetimes of 4F9/2 -4I15/2, 4I9/2 -4I15/2, 4I11/2 -4I15/2 and 4I13/2 -4I15/2 emission bands in GeGaS glasses doped with erbium, in Proc. 18th International Conference on Transparent Optical Networks (2016).

[40] O. Henderson-Sapir, J. Munch, D. J. Ottaway, Mid-infrared fiber lasers at and beyond 3.5 μm using dual-wavelength pumping, Opt. Lett. 39(3) (2014) 493-496.

[41] R. S. Quimby, B. G. Aitken, Multiphonon energy gap law in rare-earth doped chalcogenide glass, J. Non. Cryst. Solids 320(1–3), (2003) 100–112.

[42] A.B. Seddon, D. Furniss, Z. Q. Tang. L Sojka, T. M. Benson, True mid-infrared Pr3+ absorption cross-section in a selenide-chalcogenide host-glass. in Proc. 18th International Conference on Transparent Optical Networks (2016).

[43] S. R. Bowman, J. Ganem, B. J. Feldman, A. Q. Kueny, Infrared laser characterisatics of praseodymium-doped lanthanum trichloride, IEEE J. Quantum. Elect. 30 (12) (1994), 2925-2928.